Highly efficient removal and sequestration of Cr(VI) in confined MoS_2 interlayer Nanochannels: Performance and mechanism

Research article

Submitted to

Separation and Purification Technology

Qi Han[1], Julie Yu[2], Julie Yu[2], Leeann Sun[2], Minerva Teli[2], Bei Liu[1], Hong Chen[1], Kunkun Wang[1], Zhongying Wang[1,2*], Baoxia Mi[2*]

[1]Guangdong Provincial Key Laboratory of Soil and Groundwater Pollution Control, School of Environmental Science and Engineering, Southern University of Science and Technology, 1088 Xueyuan Blvd, Nanshan District, Shenzhen 518055, PR China

[2]Department of Civil and Environmental Engineering, University of California, Berkeley, California 94720, United States

*The author to whom correspondence should be addressed.

E-mail: wangzy6@sustech.edu.cn; mib@berkeley.edu;

ABSTRACT

Environmental contamination by Cr(VI) is of particular concern because of its severe toxicity and high mobility. In this study, we employed two-dimensional MoS2 nanosheets in the removal of Cr(VI), with an emphasis on revealing the removal mechanisms, and how the compositional and structural uniqueness of 2D MoS2 nanomaterials intrinsically impact the Cr removal efficiency. Through batch experiments with dispersed nanosheets, we found that MoS2 nanosheets exhibited a high Cr(VI) removal capacity at ~1100 mg/g via a phase-dependent mechanism. Particularly, the 1T polymorph in the MoS2 nanosheets removed Cr(VI) through a redox-reaction mechanism, which was different from the adsorptive removal of Cr(VI) by MoS2 reported previously, highlighting the compositional effects on the removal mechanism and performance. More importantly, the reduced product Cr(III) was concurrently removed via precipitation and adsorption onto the MoS2 nanosheets, which could avoid the additional pH-elevation step that is typically needed in the conventional treatment. The unique 2D flake-like structure of MoS2 nanosheets enabled the formation of aligned and ion-accessible nanochannels, where Cr(VI) species were accommodated, reduced and sequestered. The irreversible shrinking of the nanochannels under drying modified the interior of the layer-stacked structure into confined compartments preventing the release and re-oxidation of the immobilized Cr(III). The compiled results highlight the effects of MoS2 composition and structure on the Cr removal efficiency and mechanism, which has substantial implications on future studies tailoring these unique features of 2D nanomaterials for various remediation scenarios.

Introduction

Water contamination caused by natural resources and intensified human activities has become a global concern, and brings severe health threats to human society and ecosystem [1]. Hexavalent chromium [Cr (VI)] has been particularly concerning to the public and scientists due to its acute toxicity and carcinogenicity to living organisms [2]. In the natural environment, Cr(VI) can come from the oxidation of indigenous trivalent chromium [Cr(III)] minerals and from anthropogenic activities such as tanning, metallurgy, mining, and plating [3,4]. Due to its high solubility and mobility, Cr(VI) is readily released into soil and aquatic environments, which increases the reach and severity of its impacts. In contrast to Cr(VI), the lower oxidation counterpart Cr(III) is highly insoluble, less mobile, and 1000 times less toxic [5]. However, insoluble Cr(III) can be released into the water systems by a decrease in pH or through ligand complexation [6], and then re-oxidized feasibly to toxic Cr(VI) in redox reactions with environmental species (e.g. MnO2 or O2) that are common in ambient conditions [7-9]. Additionally, Cr(III)- containing corrosion scales in drinking water distribution pipelines can be oxidized by disinfectant chlorine and its derivatives during the water treatment processes [10]. Because of the interconvertible nature and severe toxicity of Cr species, the US Environmental Pollution Agency recommends the maximum contaminant limits (MCL) of total Cr in drinking water to be 0.1 mg/L, while the state of California sets the MCL for the toxic Cr(VI) at 0.01 mg/L.

The conventional technology for Cr(VI) remediation is initiated by the reduction of Cr(VI) to Cr(III) at low pH conditions, followed by elevation of pH to neutral conditions to precipitate Cr(III) [11,12]. Such a process requires the addition of a vast amount of chemicals and costly treatment of the secondary sludge. In the past few decades, various nanomaterials (e.g. nanoscale zero-valent iron (nZVI), MXenes and metal organic frameworks) have been employed to synchronously reduce Cr(VI) and adsorb Cr(III) [13-21]. However, challenges associated with nanoparticle aggregation, surface passivation, and tedious separation need to be addressed before full-scale application. Thus it is desirable to employ novel nanomaterials that are not plagued by the problems traditional nanomaterials face, to effectively remove and immobilize Cr species.

Two-dimensional molybdenum disulfide (MoS2) is an emerging functional nanomaterial in environmental applications, such as membrane separation [22,23], disinfection [24], and heavy

metal remediation [25,26]. MoS2 nanosheets have been widely studied as a potential adsorbent material exhibiting high selectivity and removal capacities for various toxic heavy metal cations because of the strong interaction between the S atom and heavy metal ions. (e.g. Pb2+, Hg2+) [26-33]. For oxyanion removal (e.g. CrO4 2-, AsO3 -), the reports employing exfoliated MoS2 nanosheets are rare except for a few that worked with MoS2 composite materials (e.g. with layered double hydroxide [34], Fe3O4 [35,36], polymers [37-39], and carbon [40]). Consequently, a large variation of Cr removal capacities (~70 to 320 mg/g) [34-37,41] and multiple removal mechanisms on MoS2-based composites including electrostatic attraction [34,38], ion exchange [36], surface complexation [34], and reduction [37] were reported in the literature. For instance, metallic 1T- and semiconducting 2H-MoS2 exhibit octahedral and trigonal prismatic configurations (Fig. 1a), respectively, and these characteristics have been found to be closely related with heavy metal removal efficiency [42,43]. The intrinsic interactions of Cr(VI) anions with MoS2 owning various structures and phase compositions have yet been completely understood, and this missing information is critically related to the removal mechanism, implementation approach, and the fate of remediation products.

Additionally, MoS2 nanosheets with distinct phase composition and structure can be prepared through different synthetic routes. For instance, the flake-like MoS2 nanosheets with high aspect ratio and specific surface area can be prepared by chemical exfoliation method [44]. Meanwhile, after chemical exfoliation, the 2H phase bulk MoS2 would partially convert to 1T phase, which generated MoS2 nanosheets that contained both 1T and 2H phase, allowing the study of compositional impacts on the removal and sequestration of Cr species [45]. In addition, MoS2 can be assembled into layered-stacked structures by means of vacuum filtration. This aligned layer-stacked structure can form stable nanochannels between adjacent layers, which was beneficial to the sequestration of toxic species in the confined space. [46-48].

In this study, we systematically investigated the interactions and reaction mechanisms of Cr species with chemically-exfoliated MoS2 nanosheets. The removal performance and mechanisms were studied in batch experiments, while Cr species (hexavalent and trivalent) concentrations, together with morphological and compositional evolution of MoS2 nanosheets, were carefully monitored via various characterization tools. To avoid the release of dispersed nanomaterials during remediation, MoS2 nanosheets were assembled into stable layer-stacked structures

106 containing aligned and ion-accessible nanochannels, and the effects of these nanochannels on the
107 removal efficiency and sequestration of toxic Cr species were studied.

108 **Experimental Section**

109 **Preparation of 2D MoS_2 nanosheet suspension.** Bulk MoS_2 powders (particle size ~ 2 μm) were
110 purchased from Sigma-Aldrich (Saint Louis, MO). A chemical exfoliation method was used to
111 prepare individual MoS_2 nanosheets according to the procedure reported previously.[1] Typically, 1
112 g of MoS_2 was added to 10 mL of n-butyllithium (1.6 M, Sigma-Aldrich) in hexane solution, and
113 the formed suspension was stirred in N_2-filled glove box for 48 h. The resulting lithium-
114 intercalated MoS_2 was separated by centrifuge and added with degassed deionized (DI) water for
115 forced hydration to generate monolayer MoS_2 nanosheets dispersion, which was purified by
116 dialysis in DI water using 3.5K MWCO Dialysis tubing (Thermo Scientific, Saint Louis, MO).
117 The concentration of MoS_2 dispersion was determined by digestion in 500 mM H_2O_2, followed by
118 measurements of soluble Mo concentration using inductively coupled plasma optical emission
119 spectroscopy (ICP-OES, Agilent 720, Agilent Technologies, Santa Clara, CA).

120 **Removal of Cr(VI) by dispersed MoS_2 nanosheets.** MoS_2 nanosheet suspension was directly
121 employed in the removal process of Cr(VI) without additional modification. A stock solution of
122 1000 mg/L Cr(VI) was prepared by dissolving $K_2Cr_2O_7$ in DI water. MoS_2 stock solution was
123 spiked to 20 mL of aqueous Cr(VI) solution of various concentrations, and the suspension mixture
124 was placed on a rotatory mixer at a speed of 50 rpm. At selected time points, the supernatants were
125 filtered through 0.22 μm PES syringe filters and the remaining Cr(VI) concentration was
126 determined with the 1, 5-diphenylcarbazide (DPC) method (the details provided in Supporting
127 Information) using a UV-Vis Spectrophotometer (Genesys 10S, Thermo Scientific, CA).[2] The total
128 soluble Cr concentration was determined by ICP-OES, and the Cr(III) concentration was thus
129 obtained by subtracting the concentration of Cr(VI). To study the influence of pH on the Cr(VI)
130 removal, solutions with different pH values were prepared with HCl (pH 2), acetate buffer (pH 4),
131 and MES buffer (pH 6), respectively. The reacting products of MoS_2 with Cr(VI) were collected
132 with centrifugation or filtration, washed twice with the background electrolyte, and dried in N_2 for
133 further analysis.

134 **Sequestration and release of Cr(III) in MoS_2 nanochannels.** Layer-stacked MoS_2 with aligned
135 nanochannels was prepared by vacuum filtration of nanosheet suspension containing 4 mg MoS_2

136 on the top of a poly(ether sulfone) (PES) ultrafiltration substrate. The layer-stacked MoS_2 was
137 either directly subjected to the reaction with Cr(VI) (5 mg/L, 40 mL) at pH 4 for 1 day, or a
138 complete oven-drying before the same Cr(VI) treatment, and the samples obtained were referred
139 to as stacked-wet and stacked-dry samples, respectively. As control tests, MoS_2 suspension
140 containing 4 mg sample were firstly reacted with Cr(VI) solution at the same condition, and then
141 subjected to filtration to collect the randomly-aggregated MoS_2-Cr samples on PES membranes.
142 The samples were either maintained in solutions or subjected to complete oven-drying, and thus
143 referred to as randomly-aggregated wet and dry samples, respectively. After Cr sequestration, all
144 four types of MoS_2-Cr samples were immersed in the petri-dish containing 40 mL of pH 2 HCl
145 solution, and sampling were taken at selected time to monitor the extent of Cr(III) release.

146 **Characterization.** The monolayer feature and lateral dimension of MoS_2 nanosheets were
147 revealed using a transmission electron microscope (TEM; JEOL 2100F) at an acceleration voltage
148 of 200 kV. The nanosheet thickness was obtained by atomic force microscopy (AFM) imaging
149 recorded using Bruker Icon AFM (Bruker, Billerica, MA) in non-contact mode. The cross-
150 sectional image of layer-stacked MoS_2 was recorded by a field emission scanning electron
151 microscope (SEM; Zeiss Gemini Ultra-55, Jena, Germany). Before the SEM imaging, samples
152 were coated with thin layer of gold to increase conductivity. The Grazing incident X-ray diffraction
153 data were collected at Stanford Synchrotron Lightsource (SSRL) beamline 2-1 with CCD detector
154 under refection mode, with a grazing incident angle of 2 degree, the X-ray energy is 12.7 keV. The
155 data reduction was performed with WxDiff software and calibrated with LaB6 standard. X-ray
156 photoelectron spectroscopy (XPS) surface survey and high-resolution scans were performed using
157 a Thermo Scientific K-Alpha XPS. The zeta potential and hydrodynamic size measurement of
158 exfoliated MoS_2 nanosheets were performed using NanoBrook Omni (Brookhaven, U.S.A.)

159

160 **Results and Discussion**

161 *3.1. MoS2 characterization* The MoS2 nanosheets were obtained through lithium-intercalation and
162 forced hydration of bulk MoS2 powder (Fig. S1) as reported previously [49,51]. The flake-like
163 structure of exfoliated MoS2 nanosheets was revealed in the AFM (Fig. 1b) and TEM images (Fig.
164 1c). The line profiles in Fig. 1b show that the average thickness of MoS2 nanosheets was
165 approximately 1.1 nm, consistent with the value of monolayer MoS2 reported [49]. The lateral

166 dimension of individual nanosheets was in the range of 200 to 500 nm, as shown in Fig. 1c, in line
167 with average hydrodynamic size of 250 nm (Supplementary Information Fig. S2). The zeta
168 potential of exfoliated MoS2 was found to be ~-20 to -50 mV over the pH range of 2 to 10 (Fig.
169 S3), consistent with the high colloidal stability of MoS2 suspension in a wide pH range. The MoS2
170 nanosheets also had a high chemical stability, and the suspension underwent slight oxidation at pH
171 2 with less than 1% of Mo released as soluble species within 1 d (Fig. S4). The phase composition
172 of as-prepared MoS2 nanosheets was characterized using Raman spectra, XPS and UV–vis
173 absorption, since the reactivity, stability, and interactions of MoS2 with heavy metals have been
174 associated with phase compositions [42,43,52,53]. The characterization on the phase of bulk MoS2
175 was shown for comparison. In the UV–vis absorption spectra (Fig. S5), two typical absorption
176 peaks located at 613 and 660 nm were characteristic to 2H phase and only observed for bulk MoS2.
177 The presence of 2H phase in the bulk MoS2 was also confirmed by the Raman spectra (Fig. 1d),
178 which displayed characteristic Raman shifts of the 2H phase at ~380 cm□ 1 and 410 cm□ 1 for
179 the E2g and A1g modes, respectively. For as-exfoliated single layer MoS2, characteristic peaks
180 associated with the 1T phase (i.e. J1, J2, E2g, J3) were observed at ~146 cm□ 1, 180 cm□ 1, 280
181 cm□ 1, 340 cm□ 1, indicating the mixed phase of 1T and 2H in the MoS2 nanosheets. The phase
182 composition was semi-quantitatively measured by the XPS (Fig. 1e and Fig. S6). Relative to the
183 bulk MoS2, the Mo and S peaks of the as-exfoliated nanosheets shifted towards lower binding
184 energy (~0.6 to 0.9 eV) due to the presence of 1T-MoS2 in the exfoliated product. Based on the
185 deconvolution results (Fig. 1e), the 2H and 1T components made up approximately 40% and 60%,
186 respectively, in the as-exfoliated MoS2 nanosheets. It is important to note that the peaks of
187 oxidized molybdenum (Mo5+ and Mo6+) or sulfur (S6+) were not present, which typically reside
188 at ~235–236 eV and 168–172 eV in the XPS spectra, respectively [54]. The absence of these peaks
189 indicates the high purity of exfoliated MoS2 samples, and that oxidative evolution of MoS2, if any,
190 is solely caused by redox reactions during the Cr(VI) remediation process (*infra vide*).

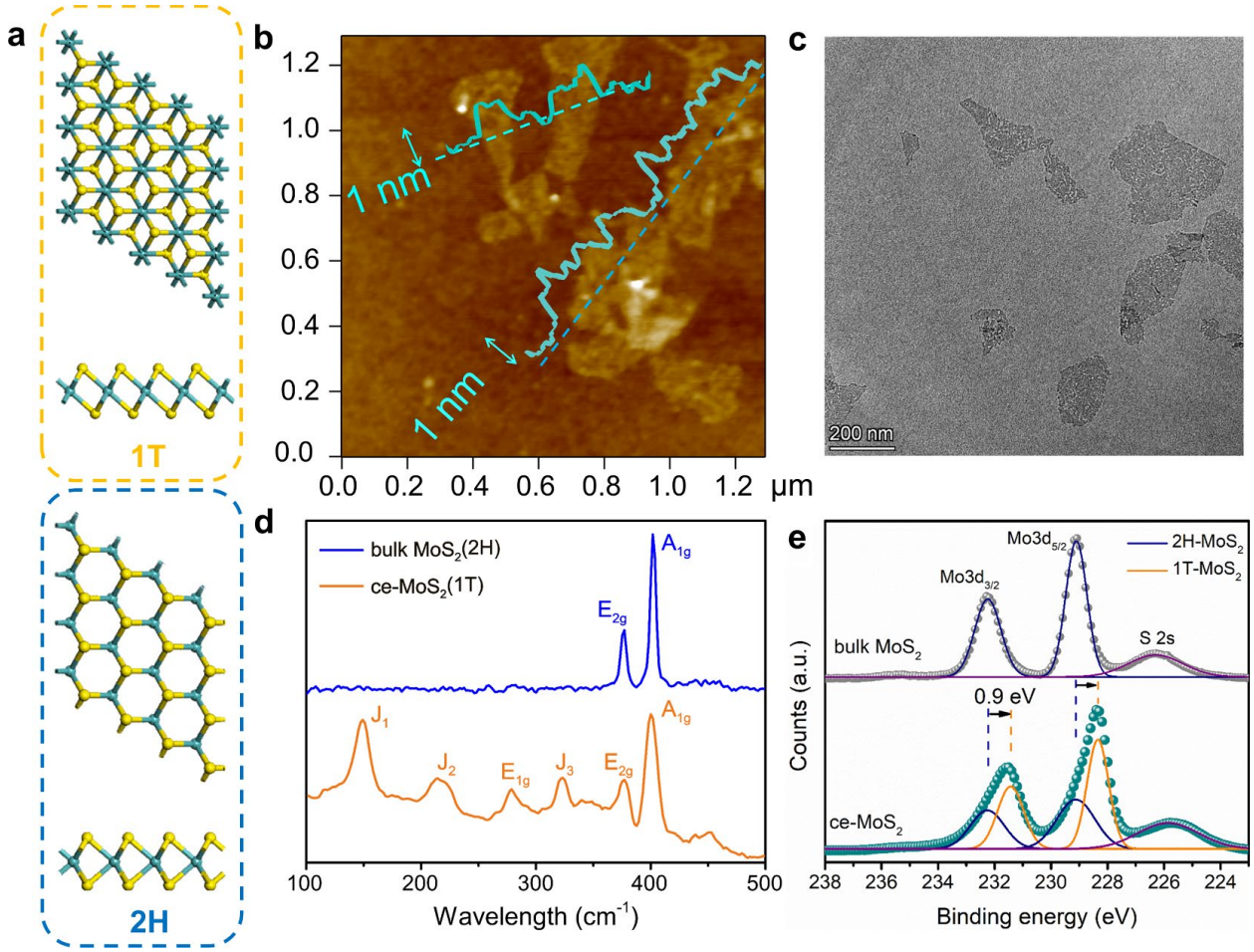

Fig. 1. Characterization of chemical exfoliated MoS2 nanosheets and bulk MoS2. (a) Structure illustration of 1T- and 2H-MoS2 (yellow ball for S atom and blue ball for Mo atom) (b) AFM image of ce-MoS2 nanosheets, with inset line scans showing the thickness profiles; (c) HRTEM image of ce-MoS2 nanosheets; (d) Raman spectra of bulk and ce-MoS2; and (e) XPS spectra of Mo 3d core level peak regions of bulk (grey) and ce-MoS2 (green).

3.2. Cr species removal by MoS2 nanosheet suspension Batch experiments were conducted to investigate the removal efficiency of Cr(VI) by MoS2 nanosheets. Fig. 2a shows that the overall Cr (VI) removal by MoS2 nanosheets was enhanced with increasing equilibrium Cr(VI) concentration at pH 2, and approached a constant capacity of approximately 1100 mg/g, which is much higher than the typical values (~100 to 250 mg/g) for Cr(VI) removal by other nanomaterials reported previously (Table S1). The superb remediation performance of MoS2 nanosheets found here and towards other heavy metals can be attributed to the excellent dispersity and abundant active sites of the exfoliated nanosheets. To investigate Cr(VI) removal kinetics, excess Cr(VI) was added into MoS2 suspensions at various pH conditions. As shown in Fig. 2b, the concentration of Cr(VI) decreased rapidly at pH 2 and the removal was almost completed with remaining Cr(VI)

at ~35 mg/L after 1 d. At pH 4 and 6, MoS2 nanosheets achieved comparable removal efficiency of Cr(VI) to that at pH 2, albeit with much slower reaction kinetics. The co-existing experiment (Fig. 2c) indicated that 50 mg/L Cr(VI) was removed completely after 24 h for each MoS2 suspension, and different anions had nearly no influence on Cr(VI) removal. The excellent adaptability of Cr(VI) removal by MoS2 to a wide pH range is of significant importance since the pH adjustments required by conventional methods consume a large amount of chemicals and need additional equipment [55]. To explore if Cr(III) is present, the concentrations of reductively generated Cr(III) species at different pH conditions were acquired by subtracting the amount of remaining Cr(VI) from the total Cr measured by ICP-OES. As shown in Fig. 3a, Cr(VI) removal was enhanced at acidic conditions and meanwhile Cr(III) was observed with higher concentrations at lower pH, which implies a redox reaction occurring between Cr (VI) and MoS2 nanosheets. In particular, complete removal of Cr(VI) and concurrent generation of Cr(III) with the same concentration (~50 mg/ L) was achieved at pH 2, which implies Cr(VI) reduction is the only removal mechanism of Cr(VI) by MoS2 nanosheets at this condition. The potent Cr(VI) reduction favored at low pH conditions can be explained by the stronger oxidation strength of Cr(VI) at acidic solutions (φCr(VI)/Cr (III) ≈1.05 V at pH 2 vs. 0.087 V at pH 8.9, according to Nernst equation). In contrast, at pH 8.9, Cr(VI) concentration didn't change considerably in the presence of MoS2 nanosheets, implying Cr(VI) can neither be reductively removed, nor adsorbed by MoS2 nanosheets at basic conditions. The weak Cr(VI) removal at pH 8.9 can be attributed to low oxidation power and anionic nature of CrO42-, making it difficult to react or adsorbed by negatively charged MoS2 nanosheets. It is worth noting that certain loss of total Cr was found at pH 4 and 6. At these conditions, the main species of Cr(VI) was HCrO4 - (Fig. S7), considering the repulsive force between anionic Cr(VI) and MoS2 nanosheets, we believe this portion of Cr was the Cr(III) that were removed along with the reacted MoS2 from the solution. The complete Cr removal via concurrent Cr(VI) reduction and Cr(III) sequestration has important implications, since this one-step removal circumvents the pH alleviation to precipitate Cr(III) required by conventional treatment approaches employing materials such as scrap iron [56], Fe(0) [57], and maghemite [50]. To confirm the concurrent removal of reductively generated Cr(III) from the aqueous solutions, we conducted additional tests and plotted the distributions of Cr species, that is remaining Cr(VI), soluble Cr(III), removed Cr(III), as functions of initial Cr(VI) concentrations at various pH conditions. As shown in Fig. 3b, the reduction of Cr(VI) by MoS2 nanosheets was

more pronounced at pH 2, but the reduced Cr(III) predominantly existed as soluble species that were retained in the solution at this condition. At pH 4 and 6, with the increase of the initial Cr(VI) concentration, a decreasing order was obtained for both the percentages of removed and soluble Cr(III) among total Cr, and the portions of remaining Cr(VI) increased. Among the Cr (III) species, most of Cr(III) were removed from the solutions at higher pH conditions. Particularly, the reduced Cr(III) were completely sequestered at pH 6 despite the comparatively less pronounced reduction of Cr(VI) because of the weak redox activity. Additionally, a control test was conducted to demonstrate the pH effect observed above did not stem from the different anions used in various buffer solutions (Fig. S8). Overall, MoS2 nanosheets exhibited excellent performance in both Cr (VI) reduction and Cr(III) sequestration at pH 4, which renders this condition as the best for removing the total Cr from solutions with a maximum capacity at ~540 mg/g.

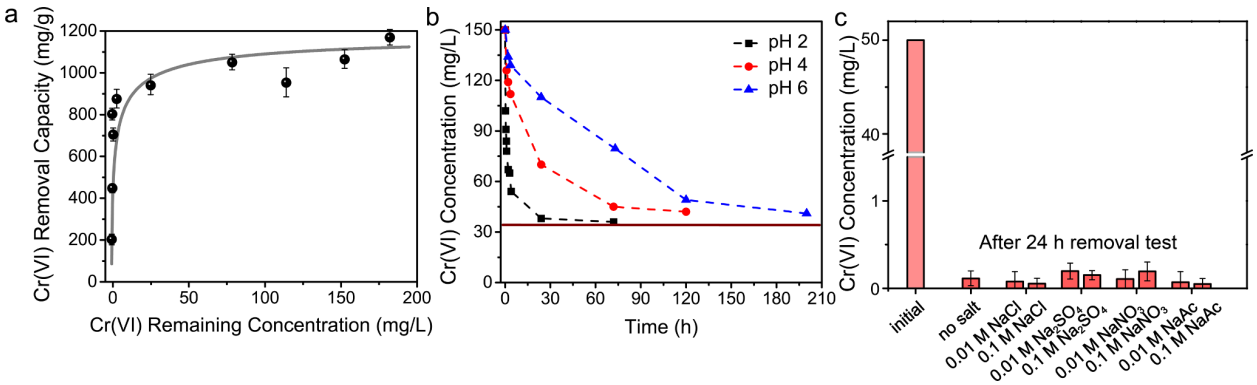

Fig. 2. Cr(VI) removal by MoS2 nanosheet suspension. (a) Cr(VI) removal capacities at various equilibrium Cr(VI) concentrations at pH 2; (b) removal kinetics of Cr (VI) at pH 2, 4 and 6; the initial Cr(VI) and MoS2 concentrations in (b) were 150 and 100 mg/L, respectively, and the red solid line in (b) represents the theoretical remaining Cr(VI) concentration according to the Eq. (1); (c) co-existing experiment of Cr(VI) removal at pH 2 in solution containing NaCl, Na2SO4, NaNO3, NaAc with concentrations of 0.01 and 0.1 mol/L, initial Cr(VI) concentration was 50 mg/L.

3.3. Removal mechanism of Cr species by MoS2 nanosheets A series of characterization and tests have been conducted to unravel the mechanism between MoS2 and Cr(VI) species. To corroborate the detection of reduction product Cr(III), the concentrations of the possible oxidation products SO42- and MoO42- were monitored and shown in Fig. 4a and 4b, respectively. The oxidative release of SO42- was enhanced with the increase of Cr(VI) concentration and the decrease of pH, in agreement with the results showing that Cr(VI) was favorably removed at lower pH conditions (Fig. 3a). The release profile of the other oxidation product MoO42- exhibited an apparently

265 different behavior from that of SO42- (Fig. 4b, S9). Despite of considerable amount of MoO42-
266 released at pH 2, the oxidized MoS2 barely exhibited detectable amounts of MoO42- if any into
267 the solutions in contrast to the appreciable SO42- generation at pH 4 and 6 (Fig. 4a and 4b).
268 Considering the total Cr loss observed in Fig. 3a, the inhibited release of MoO42- was likely caused
269 by the concurrent Cr(III) adsorption onto oxidized MoS2 and/or precipitation of Cr (III) with the
270 generated MoO42-. The precipitation could also effectively avoid the potential release of soluble
271 Mo species, which may be concerned with as secondary contaminant [58]. To validate the
272 precipitation of Cr(III) with MoO42-, Na2MoO4 and Cr (NO3)3 solutions were mixed at different
273 pH to observe the remaining Cr (III) and MoO42- concentrations. After 24 h, the concentrations
274 of MoO42- and Cr(III) decreased sharply at pH 4 and 6 but remained constant at pH 2 (Fig. S10).
275 Additionally, at pH 4 and 6 green precipitation was generated at the bottom of the vial and XPS
276 spectra implied the formation of Cr2(MoO4)3 (Fig. S11). At pH 2, MoO42- undergoes protonation
277 to form H2MoO4 (a binary weak acid), which inhibits the precipitation with free Cr3+ [59]. To
278 testify if Cr(III) could be removed by MoS2 nanosheets, we also measured the removal isotherm
279 of Cr(III) by MoS2 nanosheet suspension, which shows moderate removal capacities of 40 and
280 180 mg/g at pH 4 and 6, respectively. Nearly no adsorption of Cr(III) by MoS2 occurred at pH 2.
281 (Fig. S12), which can be explained by the low zeta potential of MoS2 nanosheets at pH 2 and thus
282 weakened the electrostatic attractions between MoS2 nanosheets and Cr(III). Collectively, the
283 reductively generated Cr(III) could be readily removed via precipitation and adsorption onto MoS2
284 nanosheets. To corroborate with ion release profiles, the MoS2 samples after Cr (VI) remediation
285 at various pH conditions were subjected to XPS characterization. XPS survey scan in Fig. S8
286 shows O and Cr peaks were barely observed in the reacted MoS2 sample at pH 2, in line with the
287 weak association of Cr(III) with the oxidized MoS2. Cr 3p XPS core level spectra indicated that
288 the adsorbed and precipitated Cr species at pH 4 and 6 were Cr(III) only (Fig. S13), and confirmed
289 the adsorption of Cr (VI) was not a feasible way in the case of MoS2 nanosheets used in this study.
290 The time-resolved Cr XPS also indicated the Cr(III) generation process at pH 4 (Fig. S14). It is
291 interesting to note that the Mo 3d XPS spectra exhibited a significant difference in MoS2 samples
292 formed at various pH conditions (Fig. 4c). The deconvolution analysis of these Mo 3d peaks
293 revealed the portions of 1T-MoS2, 2H-MoS2, and oxidized Mo, highlighted in red, blue and
294 orange, respectively. Compared to the 1T-phase-dominated pristine MoS2 nanosheets (Fig. 1e),
295 2H-MoS2 became the dominant Mo species after the reaction with Cr(VI) at pH 2 and

consequently the ratio of 1T/2H was decreased to ~0.28 (vs. ~2 in the pristine MoS2 nanosheets). This 1T/2H ratio was varied much less pronouncedly at pH 4 and 6 and determined to be ~1.2 and 1.9, respectively. Collectively, the varied 1T/2H ratios indicate that 1T-MoS2 reacted with Cr(VI) favorably over 2H-MoS2. EDS mapping (Fig. S15, Table S2) also supports the association of Cr(III) with reacted MoS2 samples at pH 4 and 6 since the Cr and O contents were apparently enhanced relative to those of the reacted MoS2 formed at pH 2. To confirm the phase effect in the removal process, we carried out time-resolved XPS and monitored the evolution of each phase during the reaction with Cr(VI) (Fig. S16). Compared to the pristine nanosheets containing 60% 1T MoS2, the percentage of 1T polymorph in the MoS2 decreased to 34, 25, 18, 13 and nearly 0 %, after the reaction with Cr(VI) for 15 min, 30 min, 2 h, 4 h and 1 d, respectively (Table S3). The reacted 1T-MoS2 was converted to oxidized Mo(VI) in the form of Cr2(MoO4)3 or Mo oxide.

On the other hand, the reaction rate between 2H-MoS2 and Cr (VI) was much slower if any, maintaining the percentage of 2H phase at approximately 40% of the total Mo in the MoS2 solids throughout the entire reaction. This is consistent with the higher chemical stability of the 2H-MoS2 polymorph relative to the 1T-MoS2 polymorph observed in previous studies [43,52]. We also tested the reaction between Cr(VI) with bulk MoS2 containing only 2H phase, and the Cr(VI) concentration didn't decrease within 1 d (Fig. S17), which confirmed that the reaction rate of 2H-MoS2 with Cr(VI) is very slow, if any. In the time-resolved evolution of S 2p XPS spectra (Fig. S19), the position shift towards higher binding energy confirms the preferential decomposition of 1T polymorph. Additionally, the absence of the oxidized S peak at ~168 eV corroborates the release of oxidative product SO42- from MoS2 surfaces as discussed above.

The efficient removal of Cr(VI) from solution observed in this study is thus attributed to Cr(VI) reduction by MoS2 nanosheets (1T primarily), concurrent Cr(III) precipitation and adsorption on oxidized MoS2 nanosheets (Fig. S18), which can be described by the following equations:

$$\equiv MoS2(1T)+6HCrO\square 4+6H2O \rightarrow MoO42\square +6Cr3+ +18OH\square +2SO2\square 4 \quad (1)$$

$$3MoO42\square +2Cr3+ \rightarrow Cr2(MoO4)3 \quad (2)$$

$$\equiv MoS2 +Cr3+ \xrightarrow{\equiv} adsorption \equiv MoS2 \square Cr \quad (3)$$

The concomitant precipitation and adsorption of Cr(III) after the reduction of Cr(VI) is important since the adsorptive removal of hydrated Cr(III) ions has been reported to be slow and difficult

325 due to the kinetic inertness of water exchange [60,61]. Based on Equation (1), the maximum Cr(VI)
326 reductive removal capacity of MoS2 nanosheets can be calculated to be 1170 mg/g (see details in
327 SI Text), granted that only the 1T component is completely oxidized while 2H-MoS2 remains
328 intact. The calculated values are plotted in Fig. 2b for comparison, exhibiting strong consistency
329 with the Cr(VI) removal capacity determined by batch experiments.

330 The as-exfoliated MoS2 nanosheets have a nearly 1100 mg/g redox capacity of Cr(VI). This value
331 is much higher than those for MoS2 synthesized through other methods and for MoS2 composites,
332 which reached the capacity of ~70 to 290 mg/g for 2H phase [34-36] and ~290 to 320 mg/g for 1T
333 phase [37,41], highlighting the importance of MoS2 phase and structure on the removal efficiency
334 of Cr species. For exfoliated MoS2 monolayers, the good dispersity and monolayer structure also
335 renders the maximum exposure of active sites leading to high removal efficiency of total chromium
336 by MoS2 nanosheets. The extraordinary total Cr removal performance of MoS2 nanosheets at
337 near-neutral pH outperforms peer nanomaterials, in which a vast amount of chemical usage is
338 needed to adjust pH.

339 *3.4. Confined nanochannels in layer-stacked structure* After demonstrating the Cr removal
340 mechanism and efficiency with dispersed nanosheets, we assembled MoS2 individual sheets into
341 macrostructures to (1) circumvent the subsequent burden of nanomaterial separation potentially
342 encountered in practical remediation, and (2) to reveal the structural uniqueness of 2D
343 nanomaterials applicable to influencing the environmental fate of target contaminants. Herein, we
344 prepared layer-stacked MoS2 macrostructure (Fig. 5a) *via* vacuum filtration of MoS2 suspension
345 according to our previous study [62]. Well-aligned nanochannels were formed between
346 neighboring layers held tightly *via* the van der Waals force. These nanochannels in solution
347 exhibited a stable interlayer spacing at ~1.1 nm (equivalent to 0.8 nm free spacing [62], as
348 demonstrated by the characteristic GIWAXS peak at 5◦ in Fig. 5b. Stability of the interlayer
349 spacing was maintained in an equilibrium between attractive van der Waals force and repulsive
350 hydration force [62]. Due to the smaller ionic radius of Cr(VI) (0.229 nm for CrO42- [63])
351 compared with MoS2 nanochannels, we found that layer-stacked MoS2 structures could maintain
352 highly effective removal of Cr (VI) and concurrent adsorption of Cr(III). Similar to dispersed
353 nanosheets, layer-stacked MoS2 macrostructure reductively removed Cr(VI) much faster at low
354 pH (~2), but eventually reduced the Cr(VI) concentration from 50 mg/L to less than 0.1 mg/L at

all pH conditions tested. At pH 6, soluble Cr(III) was not detected throughout the entire Cr (VI) removal process. At pH 2 and 4, concentrations of Cr(III) increased overtime and reached constant values of ~48 and 12 mg/L, amounting to 98 % and 24 % of total Cr, respectively. The adsorbed Cr(III) can also be readily released by the incubation at pH 1 HCl solutions to regenerate the MoS2 membrane (Fig. S20). In the consecutive cycles, Cr(VI) can be removed completely within a day and the remaining total Cr concentration was less than 0.1 mg/L, lower than the MCL of total Cr in drinking water guided by US EPA.

Sorbate desorption is usually desired for sorbent recyclability and resource recovery. However, sequestration is preferred when the concerned adsorbed species are highly reactive, acutely lethal, and/or radioactive. In the case of Cr, a decrease in pH or the presence of organic ligands can release the adsorbed Cr(III), which can be re-oxidized to toxic Cr(VI) by oxidative species (*e.g.* MnO2, O2) present in the natural environment [7]. Herein, we demonstrate a new toxic ion sequestration strategy by using the nanochannels in layer-stacked MoS2. As shown in Fig. 5c, wet layer-stacked MoS2 was ion-accessible and able to remove Cr (VI) *via* surface and interior active sites. Once dried in a vacuum oven at 80 ℃ overnight, these nanochannels underwent irreversible shrinking with interlayer spacing down to 0.65 nm (equivalent to ~0.3 nm free spacing, Fig. 5b), which prevented the penetration of any ionic species access inside or outside the layered-stacked structure. The narrowed spacing can't recover to > 1 nm even after the layer-stacked structure was immersed back in water solution because of the enhanced van der Waals force at sub-nanometer scale and the lacking hydration force (Fig. S21) [62].

To demonstrate the efficiency of ion-sequestration in the narrowed and confined nanochannels, we prepared layer-stacked MoS2 to reduce Cr(VI) and concomitantly adsorbed Cr(III) within nanochannels at pH 4. The Cr-loaded stacked MoS2 structures were either maintained in solution or dried in vacuum conditions overnight, followed by Cr(III) release tests at pH 1, a more favorable condition for Cr(III) release (Fig. 6a). To reveal the importance of aligned nanochannels, we also conducted control tests for comparison, in which Cr(VI) was directly added to MoS2 nanosheet suspension for reduction and Cr(III) adsorption. Due to Cr(III) adsorption and thus neutralization of negatively charged MoS2 layers, the MoS2 nanosheets agglomerated, resulting in a randomly aggregated porous MoS2 structure (Fig. S22). The aligned nanochannels were absent in the randomly assembled MoS2 structure as implied by a comparison of the XRD patterns in Fig. S21.

385 Complete Cr(VI) reduction and adsorption was achieved in both layer-stacked and randomly-
386 aggregated MoS2 samples as no Cr was detected in the remaining reaction solution of pH 4. Under
387 dry or wet conditions (Fig. 6a), the Mo and Cr release profiles at pH 1 are shown in Fig. 5b and
388 5c. Within the well-aligned nanochannels, the concentration of Cr released from the dry MoS2
389 was ~0.8 mg/L, amounting to 16 % of the total Cr loaded. The amount released under dry
390 conditions was significantly less than that from wet MoS2 (56 %) because of the irreversibly
391 narrowed nanochannels in dry MoS2 inhibiting Cr(III) ions from diffusing out (Fig. 6c). The small
392 amount of Cr released in the dry nanochannels may stem from the Cr adsorbed on the membrane
393 surface, while the majority of the Cr(III) trapped in the completely restacked nanochannels was
394 stable against release. However, in the poorly aligned porous structure, the release profiles in Fig.
395 6b show that Cr(III) was released from dry (44 % of the total Cr) and wet (50 % of the total Cr)
396 samples rapidly as a consequence of favorable release at lower pH conditions. In this case where
397 aligned nanochannels were lacking, the rate of the Cr release was quite comparable irrelevant to
398 the physical state of the porous structure. It is worth noting that the release curves of Cr and Mo
399 species follow a similar pattern in the acidic solution for the dry and wet samples in both structures,
400 which confirms the association of Cr with Mo in the oxide forms. Despite that the material
401 displayed good durability for recycling, the successful sequestration for Cr(III) by using
402 irreversible restacking of 2D layer-stacked structure paved a way for removing and isolating other
403 severely toxic (*e. g.* Hg2+) or radioactive metals, where sequestration is considered a priority over
404 recycling.

405 **4. Conclusions** As an emerging environmental remediation material, 2D MoS2 nanosheets exhibit
406 excellent Cr(VI) removal capabilities and profound interaction routines. Thanks to their
407 compositional and structural characteristics, 2D MoS2 nanosheets can concomitantly reduce,
408 precipitate and sequester toxic Cr species. Specifically, toxic Cr(VI) can be reduced by MoS2
409 nanosheets (primarily 1T polymorph) at a wide range of pH conditions from acidic to near-neutral.
410 The reductive removal capacity of Cr(VI) can reach ~1100 mg/g at all pH conditions tested. The
411 reduced product Cr(III) species can be adsorbed and/or precipitated concomitantly onto the
412 oxidized MoS2 at pH 4, which can avoid the additional usage of chemicals to elevate pH and
413 precipitate Cr(III) required by other methods. In addition, the adsorbed Cr(III) can be sequestered
414 inside the nanochannels, and the narrowed interlayer spacing caused by feasible drying can inhibit
415 Cr releasing even under environmental conditions that are favorable for Cr re-dissolution. During

the removal process, the generated MoO42- would precipitate with Cr (III) and be eliminated, which could avoid the secondary pollution. The concentration of the other released byproduct SO42- should be monitored in the practical applications, though it is a common anion in the environment with a much higher allowable concentration. This study reveals 2D MoS2 as an excellent remediation material for Cr(VI) removal, and the irreversible restacking of 2D layer-stacked structure can be further explored in future work as an approach for removing and isolating other severely toxic (*e.g.* Hg2+) or radioactive metals ions. Additionally, the impacts of the unique flake-like structure of 2D materials on their environmental applications, fate, transport and risks associated with 2D morphology should also be explored in future studies.

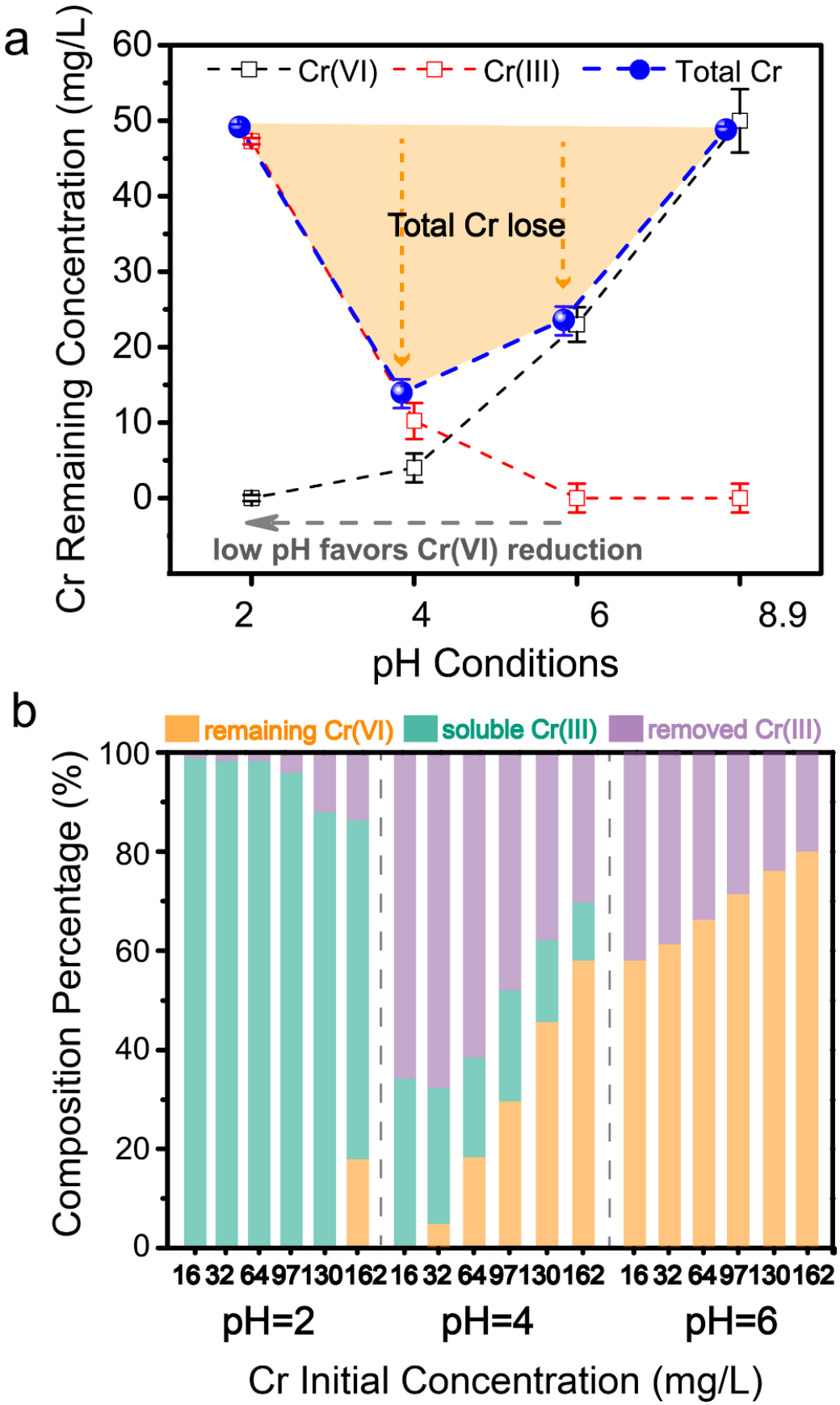
a
Cr(VI)
Cr(III)
Total Cr
Total Cr lose
low pH favors Cr(VI) reduction
Cr Remaining Concentration (mg/L)
pH Conditions
b
remaining Cr(VI)
soluble Cr(III)
removed Cr(III)
Composition Percentage (%)
pH=2
pH=4
pH=6
Cr Initial Concentration (mg/L)

Fig. 3. Removal efficiency of the total Cr by MoS2 nanosheet suspension. (a) The concentrations of total Cr, remaining Cr(VI) and reduction product Cr(III) in the reaction with MoS2 suspension over the pH range of 2 to 8.9 after 1 d (the initial concentration of Cr(VI) is 50 mg/L); (b) Remaining Cr(VI), soluble Cr(III) and removed Cr(III) percentages at different initial Cr(VI) concentrations and different pH conditions. (The initial MoS2 concentration is about 100 mg/L).

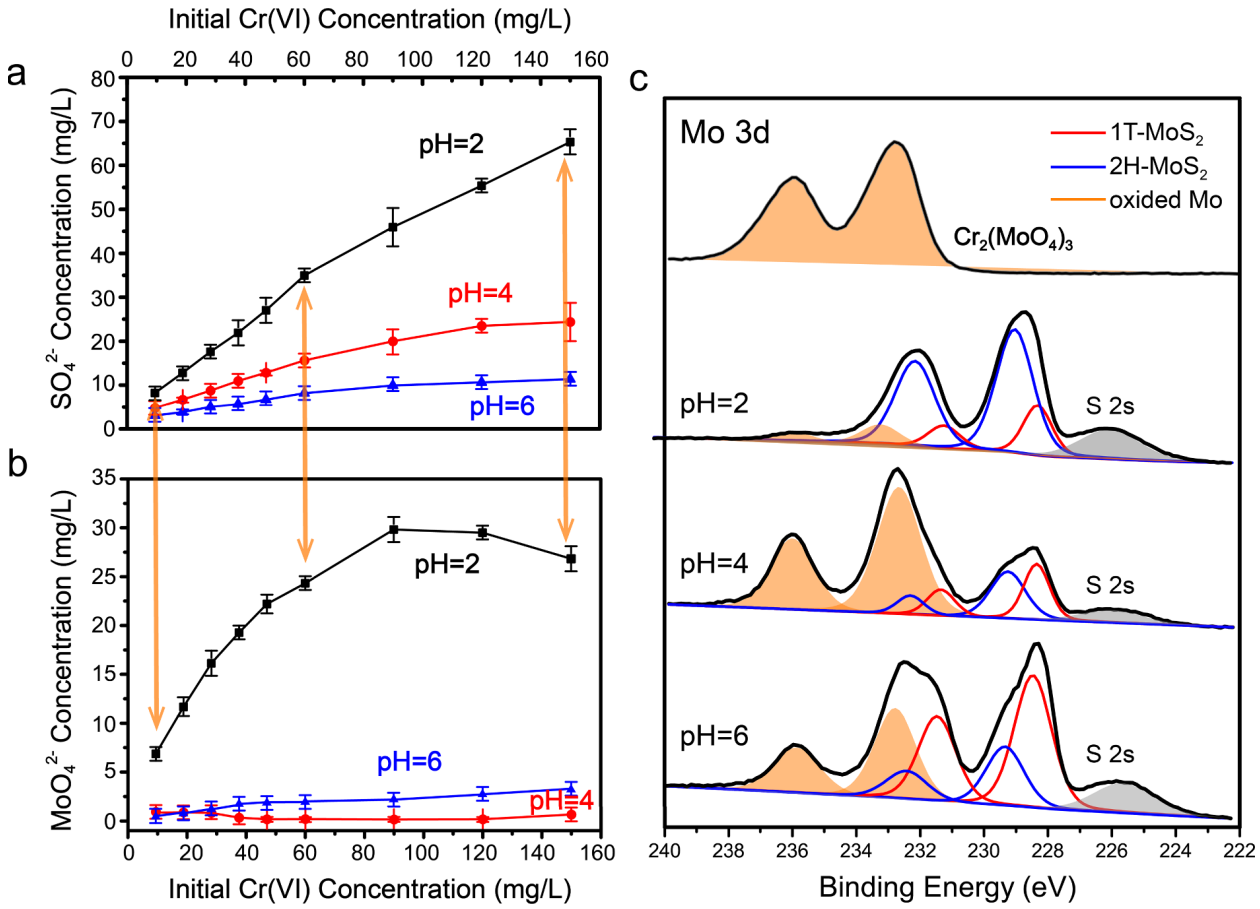

Fig. 4. Cr(VI) removal mechanism by MoS2 nanosheet suspension. Released SO42- (a) and MoO42- (b) concentrations as functions of initial Cr(VI) concentrations after reactions for 1 d at different pH; (The initial MoS2 concentration is for about 100 mg/L) (c) Mo 3d XPS spectra of Cr2(MoO4)3 as a reference and MoS2 samples in reactions with Cr(VI) at different pH.

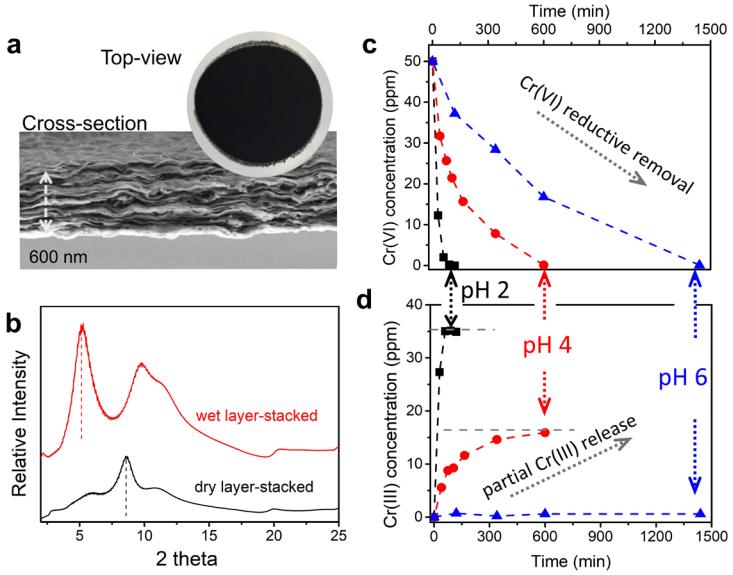

Fig. 5. Characterization and Cr(VI) removal performance of layer-stacked MoS2. (a) Cross-sectional SEM image and optical image of layer-stacked MoS2; (b) GIWAXS pattern of wet and dry layer-stacked MoS2. The radiation X-ray wavelength is 0.9765 Å, and thus peaks at 5◦ and 8.6◦ in wet and dry MoS2 samples correspond to spacing of 1.12 and 0.65 nm, respectively; (c) the remaining Cr(VI) and (d) Cr(III) concentrations of the solution containing 50 mg/L Cr(VI) and 4 mg wet layer-stacked MoS2.

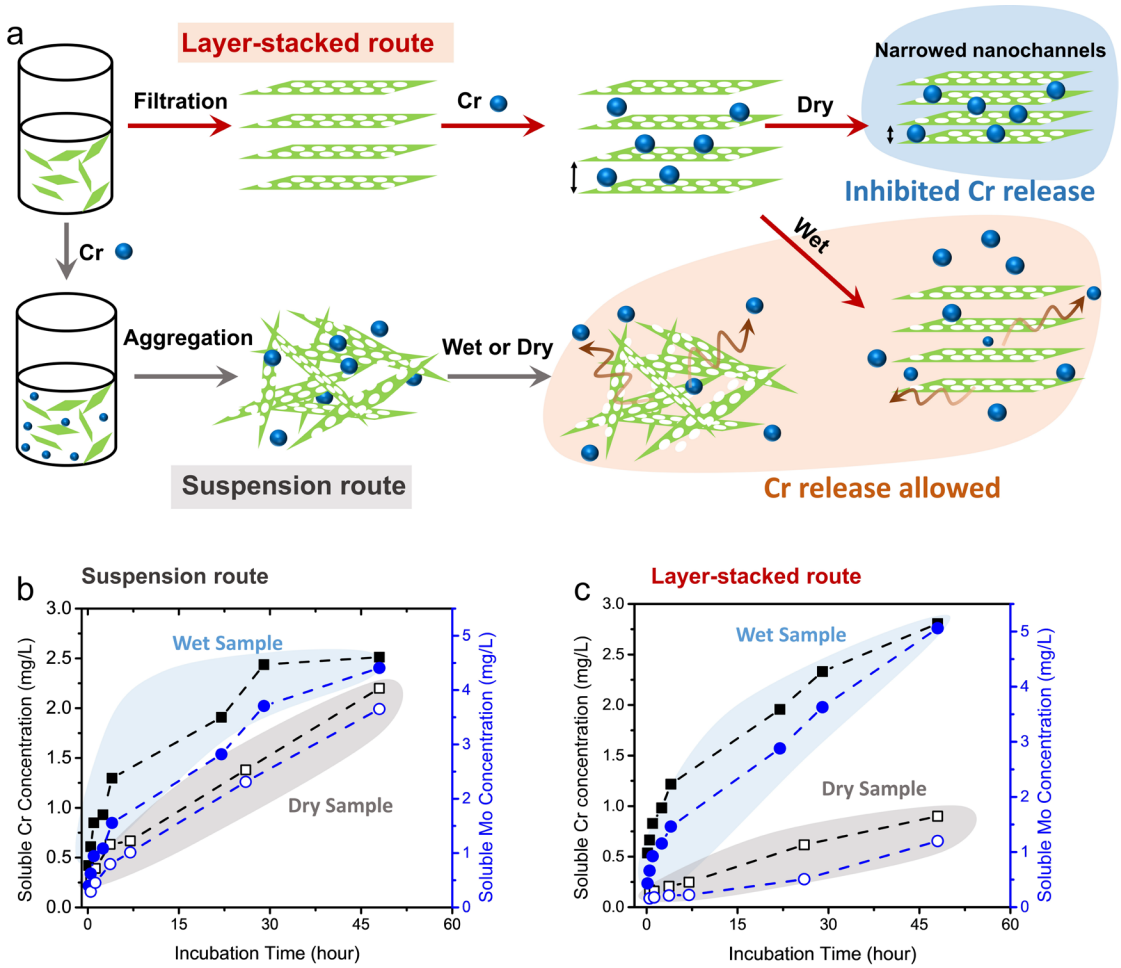

Fig.6. The sequestration effects of confined MoS_2 nanochannels against Cr(III) release. (a) Scheme of preparation and release process of well-aligned nanochannels and randomly-aggregated MoS_2; Cr and Mo species release profiles from layer-stacked MoS_2 (b) and randomly-aggregated porous MoS_2 (c). Cr(VI) species (5 mg/L) was reduced and adsorbed at pH 4, and release tests were conducted at pH 2. The "dry" samples were prepared by drying the samples in the vacuum condition overnight while "wet" samples were subjected to release test without any treatment.

Acknowledgement

CRediT authorship contribution statement **Qi Han:** Methodology, Formal analysis, Data curation, Investigation. **Julie Yu:** Writing – review & editing. **Sidney Poon:** Writing – review & editing. **Leeann Sun:** Writing – review & editing. **Minerva Teli:** Writing – review & editing. **Bei Liu:** Data curation. **Hong Chen:** Data curation. **Kunkun Wang:** Data curation. **Zhongying Wang:** Conceptualization, Data curation, Investigation, Writing – review & editing, Supervision. **Baoxia Mi:** Writing – review & editing, Supervision.

Declaration of Competing Interest The authors declare that they have no known competing financial interests or personal relationships that could have appeared to influence the work reported in this paper.

Acknowledgement The material is based upon work at UC Berkeley supported by the U. S. National Science Foundation under award nos. CBET-1565452 and CBET-1706059. Work at SUSTech was supported by National Natural Science Foundation of China (No. 22076075), Stable Support Plan Program of Shenzhen Natural Science Fundation (No.20200925155303001), SUSTech-MIT Joint Center for Mechanical Engineering Education and Research, and State Environmental Protection Key Laboratory of Integrated Surface Water-Groundwater Pollution Control. Use of the Stanford Synchrotron Radiation Lightsource, SLAC National Accelerator Laboratory, was supported by the U.S. Department of Energy, Office of Science, Office of Basic Energy Sciences under Contract No. DE-AC02-76SF00515. The authors acknowledge the assistance of SUSTech Core Research Facilities. The opinions expressed herein, however, are those of the authors and do not necessarily reflect those of the sponsors.

Reference

1. Eda, G.; Yamaguchi, H.; Voiry, D.; Fujita, T.; Chen, M.; Chhowalla, M., Photoluminescence from chemically exfoliated mos_2. *Nano Letters* **2011,** *11*, (12), 5111-5116.
2. Hu, J.; Chen, G.; Lo, I. M., Removal and recovery of cr(vi) from wastewater by maghemite nanoparticles. *Water Research* **2005,** *39*, (18), 4528-4536.